*Acta Neurochirurgica Supplementum (Journal), Suppl. 98, Springer Verlag Wien, pages 33-41, 2006*

# Uncertainty in Diffusion Tensor Based Fibre Tracking

Horst K. Hahn[1], Jan Klein[1], Christopher Nimsky[2], Jan Rexilius[1], and Heinz-Otto Peitgen[1]

1. MeVis, Center for Medical Diagnostic Systems and Visualization, Bremen, Germany

2. Department of Neurosurgery, University Erlangen-Nurnberg, Erlangen, Germany

## Summary

Background: Diffusion tensor imaging and related fibre tracking techniques have the potential to identify major white matter tracts afflicted by an individual pathology or tracts at risk for a given surgical approach. However, the reliability of these techniques is known to be limited by image distortions, image noise, low spatial resolution, and the problem of identifying crossing fibres. This paper intends to bridge the gap between the requirements of neurosurgical applications and basic research on fibre tracking uncertainty. / Method: We acquired echo planar diffusion tensor data from both 1.5T and 3.0T scanners. For fibre tracking, an extended deflection-based algorithm is employed with enhanced robustness to impaired fibre integrity such as caused by diffuse or infiltrating pathological processes. Moreover, we present a method to assess and visualize the uncertainty of fibre reconstructions based on variational complex Gaussian noise, which provides an alternative to the bootstrap method. We compare fibre tracking results with and without variational noise as well as with artificially decreased image resolution and signal-to-noise. / Findings: Using our fibre tracking technique, we found a high robustness to decreased image resolution and signal-to-noise. Still, the effects of image quality on the tracking result will depend on the employed fibre tracking algorithm and must be handled with care, especially when being used for neurosurgical planning or resection guidance. An advantage of the variational noise approach over the bootstrap technique is that it is applicable to any given set of diffusion tensor images. / Conclusions: We conclude that

the presented approach allows for investigating the uncertainty of diffusion tensor imaging based fibre tracking and might offer a perspective to overcome the problem of size underestimation observed by existing techniques.

## Keywords

Neurosurgical Planning, Risk Analysis, White Matter Tracts, Fibre Tracking,
Diffusion Tensor Imaging, Bootstrap Methods

## 1. Introduction

Magnetic resonance imaging (MRI) plays a major role in neurosurgical planning and decision support by depicting lesions within their anatomical context, information that can be used in a neuronavigation system. Moreover, intraoperative MRI allows for objectively determining the extent of resection during surgery (25). Over the last five years, diffusion tensor imaging (DTI) received increasing attention in the neurosurgical community with the motivation to identify major white matter tracts afflicted by an individual pathology or tracts at risk for a given surgical approach (11, 24, 30). Colour-encoded maps of fractional anisotropy (FA) computed from intraoperative DTI were also successfully employed to depict the shifting of major white matter tracts during surgery (19).

An explicit geometrical reconstruction of major white matter tracts has become available by fibre tracking (FT) based on DTI data (18). The feasibility on intraoperative DTI data has been shown by Nimsky et al. (20). Rather than requiring manual segmentation on every image slice, FT uses the directional information of the DTI data to three-dimensionally (3D) trace major diffusion paths starting from seed points or a seed region (2, 18). The reliability of current DTI-based FT, however, is known to be limited by image distortions, image noise, low spatial resolution, and the problem of identifying crossing fibres (11, 16). Therefore,

additional functional and electrophysiological image guidance is mandatory in many cases (11).

The problem of image distortions is most often related to the use of Echo Planar Imaging (EPI) for DTI, which offers fast imaging with acceptable signal-to-noise ratio (SNR). While the possibility of distortion compensation by post-processing the images, such as intra-subject spatial alignment to a high-resolution anatomical image, is limited by the loss of image information caused by strong distortions, novel acquisition techniques promise to deliver mostly undistorted images at the cost of longer acquisition times (21).

The dependency of DTI-FT on image noise has been studied by various researchers based on theoretical consideration and numerical simulations (1, 12, 16, 27). The main finding reported in literature is the mean tract deviation to increase approximately linearly with the distance from the seed point and to decrease with increasing SNR and diffusion anisotropy within the fibre bundle (1, 12). Still, Yamada et al. (30) reported that on a standard 1.5 T whole-body scanner with parallel imaging a scan time of less than five minutes already suffices for clinically useful FT.

The dependency of the FT result on the image resolution has not been widely described so far. In most publications, a close to isotropic image resolution of approximately 1.8-2.0 mm is used to acquire the DTI data. Tournier et al. found within simulated experiments that partial volume effects have a detrimental effect for tracking narrow fibres surrounded by anisotropic background (27). Still, the question remains if and how image resolution and the corresponding partial volume effects might also afflict the tracking of larger fibre bundles. A specific effect of currently employed FT techniques is that the actual size of fibre bundles is underestimated while the direction of fibres often can be well assessed. This has been reported to be problematic when related to neurosurgical applications (11). It has to be questioned whether this underestimation is due to the limited resolution of DTI images or due to inadequacies in existing image analysis methods.

Recently, a so-called bootstrap approach (4) has been used to visualise statistical properties of a given FT method and a given image quality (9). Therein, a non-isotropic distribution of FT uncertainty has been found, such as expressed by the local orientation uncertainty, in accordance to the regions of low anisotropy or branching fibre tracts (8, 10).

The goal of this paper is to bridge the gap between basic research on FT uncertainty and neurosurgical applications and requirements. To this end, we propose an alternative method that follows the same idea as the bootstrap approach. This alternative allows in any DTI data set to assess the geometrical variability of fibre tract reconstructions corresponding to a given FT algorithm and parameterisation in dependence of image quality. Furthermore, we present an FT algorithm as an extension of the deflection-based approach by Weinstein et al. (28) with enhanced robustness to impaired fibre integrity such as caused by diffuse or infiltrating pathological processes. We apply these methods to reconstruct the pyramidal tracts in a glioma patient and parts of the posterior corpus callosum in a healthy volunteer. The data stem from a 1.5T and a 3.0T magnet, respectively. Finally, we examine in a realistic but controlled environment the effects of resolution and SNR on the FT results in order to assess the feasibility of FT on low-quality scans that might be routinely acquired by current clinical scanners in an acceptable timeframe.

## 2. Methods and Materials

### 2.1 Image Acquisition

One patient suffering from a right hemispheric glioma (F, 73 y) and a healthy volunteer (M, 31 y) are considered. For the tumour patient, echo-planar DTI data is acquired on a 1.5 T Siemens Sonata (image resolution 1.875×1.875×1.9 mm³, 60 slices, 6 gradient directions, single channel standard head coil, scanning time ~6 min., cf. Fig. 1). For the healthy volunteer, DTI data is acquired on a 3T Siemens Allegra (image resolution 1.846×1.846×1.6 mm³, 80 slices, and 30 gradient directions each, single-channel head coil, averaged over 5 repetitions,

scanning time ~13 min.). The image noise of these images can easily be determined as described by Sijbers et al. (26) and serves as basis for a comparison to the images including artificially added complex Gaussian noise, cf. Sec. 2.4.1.

<INSERT FIGURE 1 HERE>

## 2.2 Image Filtering

In many cases, DTI data is acquired using an anisotropic image resolution, i.e. the slice thickness, commonly without inter-slice gap, is larger than the in-plane pixel spacing. Thus, the highest encoded spatial frequency is larger along the x and y axis (constituting the image plane) than along the z axis (the patient's y axis, running perpendicularly to the imaging plane). In such case, if no spatial normalization is applied to the image data, FT results would depend on the fibre orientation with respect to the imaging plane. For example, a highly curved tract would be reconstructed more accurately within in the x-y plane than within the x-z or y-z planes.

Before FT, we consequently propose to discard the highest frequency content in x and y direction in order to obtain the isotropic image content from the primary image data with an isotropic voxel size equal to the original slice thickness (e.g. 0.8×0.8×2.5 mm³ is mapped to 2.5×2.5×2.5 mm³). To this end, the resolution reduction in x and y direction would ideally be performed by k-space cropping in order to maintain MR image characteristics. A good approximation to this k-space operation is resampling with a Sinc or Lanczos filter in the spatial domain. In this study, we use a three-lobed Lanczos filter separately along all three principal coordinate axes.

The isotropic MR data is then interpolated in order to provide DTI information at any spatial position. We propose to perform a supersampling of the data before FT to an isotropic target voxel size of approximately 1.0-1.5 mm using a higher-order filter in order to enhance the quality of FT results. This supersampling does not add information to the image, but allows

for using a simple tri-linear interpolation at the later tracking stage. In correspondence to the primary resampling step, supersampling would ideally be performed by zero-filling in k-space. Again, we propose to use a Lanczos-3 filter in the spatial domain that represents a good trade-off between computational speed and filtering accuracy.

In addition to spatial resampling, denoising of the original MRI data might be beneficial in case of high image noise, but also induces assumptions, which cannot be warranted in general, on the underlying signal (17). Instead of denoising, it is also common to simply smooth the data using a Gaussian filter, while the filter width is chosen empirically according to the respective SNR; larger filters for low SNR, and vice versa. We did not consider Gaussian smoothing within this study.

### 2.3 Extended Fibre Tracking Method

The FT algorithm we employed is based on the deflection-based approach by Weinstein et al. (28) and makes use of the full diffusion tensor information during tracking. In contrast, streamline-based algorithms that are commonly employed, such as the FACT (Fibre Assignment by Continuous Tracking) method (18), take into consideration only the largest eigenvector representing the main diffusion direction. In comparison to the method described by Weinstein et al. (28), we added a novel moving average estimation of the fibre curvature and anisotropy to the tracking algorithm, which leads to more accurate tracking dynamics and more robust termination criteria (23).

In most cases, FT is applied to discrete images, but the tracking algorithm leads to sub-voxel positions $r^{t}$. Therefore, we calculate the new direction for the diffusion tensor at each corner of the cube including $r^{t-1}$ and use tri-linear interpolation for the calculation of the new direction at position $r^{t}$.

Usually, the diffusion anisotropy (DA) and the curvature at the current tracking position determine whether the tracking terminates. Tracking is stopped as soon as the DA falls below

or the curvature exceeds some threshold value. These local termination criteria are highly sensitive to noise, because the FT could be trapped in a local minimum or maximum of the DA or the curvature, respectively. Furthermore, whether the FT is trapped or not at some local extremum depends unpredictably on the step size. Tournier et al. who showed that the accuracy of FT sensitively depends on the step size (27).In order to avoid this problem, we calculate moving averages of both the DA and the curvature with respect to a window on the tracked fibre.

Since on the one hand fibre bundles with high curvature are reconstructed with streamline more accurate than with deflection-based tracking and on the other hand deflection-based tracking is more robust to orientation uncertainty (OU), we set the main vector weighting equal to the curvature normalized by the maximal expected curvature.

Furthermore, we scale the weighting factors for the trilinear interpolation of the new directions at each corner of the cube including $r^{t-1}$with $(\pi/2 - \theta)$, where $\theta$ is the angle of uncertainty. This curvature and OU weighting was found to significantly improve fibre reconstruction especially at the border of simulated fibre bundles or given white matter tracts, respectively (23).

All image analysis methods used in this paper have been built upon the research and development platform MeVisLab (31).

### 2.4 Assessment of Fibre Tracking Uncertainty

Although an assessment of the FT with respect to its uncertainty is essential in clinical applications, only little work has been done in this area. In a recent paper by Jones et al. , the bootstrap method (4, 22) was used for visualizing the uncertainty of fibre orientation in conjunction with the trajectory data (10). However, their method needs several repetitions of each image that are not available in the standard setting.

To overcome this problem, we present a new method that allows for an efficient computation of diffusion weighted images with user-defined noise while retaining the MRI noise characteristics. The resulting images are used to analyse the tracking uncertainty resulting from image noise. The main idea is to add complex Gaussian noise to the magnitude images. In contrast to the bootstrap method, our technique needs only a single data set so that the amount of required original data and the time for computing the artificial data can be reduced dramatically.

### 2.4.1 Complex Gaussian Noise

The noise distribution of acquired MR images, even after 2D inverse Fourier transformation is commonly assumed to be Gaussian (26). However, after magnitude calculation the data is no more complex and the noise is Rician distributed (6). We now propose to add complex Gaussian noise to the magnitude images, so that the noise distribution is equivalent to those of standard MR images.

Given a pixel value $|\tilde{I}_{x,y}|$ of the magnitude image, we define a corresponding complex number $\tilde{C}_{x,y} = |\tilde{I}_{x,y}| + 0i$ because we can choose an arbitrary point on the circle of the magnitude, the magnitude determination of the complex MR signal $\tilde{I}$ being rotation-invariant. For the moment, let us assume we would like to add noise with a complex Gaussian distribution of width $\sigma$ to $\tilde{C}_{x,y}$. The resulting complex number is $\tilde{C'}_{x,y} = \tilde{C}_{x,y} + \tilde{N}(0, \Sigma)$, where $\tilde{N}(0, \Sigma)$ denotes a normal distributed complex number with mean 0 and covariance matrix $\Sigma = \sigma^2 E$. Thereafter, the corresponding new magnitude value can be determined as $|\tilde{C'}_{x,y}|$ (cf. Fig. 2). Now, let us assume that the MR signal $\tilde{I}$ is corrupted by Gaussian noise with variance ${\sigma_1}^2$. Further, let ${\sigma_2}^2$ denote the desired variance of the resulting image. It is well known that, if $X_1 \sim N(\mu_1, \Sigma_1)$ and $X_2 \sim N(\mu_2, \Sigma_2 - \Sigma_1)$ are independent variates, then $X_1 + X_2 \sim N(\mu_1 + \mu_2, \Sigma_2)$. As a consequence, $\sigma^2$ can simply be determined as $\sigma^2 = {\sigma_2}^2 - {\sigma_1}^2$, so that the standard deviation of the noise to be added is $\sigma = \sqrt{{\sigma_2}^2 - {\sigma_1}^2}$. The

complexity of our new approach is only in O(*s*), with *s* being the number of voxels, because all new images can be derived from the single set of existing images.

<INSERT FIGURE 2 HERE>

### 2.4.2 Visualizing the Uncertainty

Let $\sigma_2$ denote the desired noise of the images from which we would like to visualise the uncertainty. Then, the difference noise $\sigma$ can be added to the original images as described above.

For the resulting new data set, FT is performed for a (small) set consisting of *n* seed points and the streamlines are stored and accumulated within a set of streamlines *S*. This process is repeated *m* times for the same seed points resulting in a set *S* consisting of *n*·*m* streamlines.

Now, the uncertainty can be regarded as the difference between the so-called superset trajectories – the streamlines that results when we add no noise to the original images (cf. Figs. 3 and 4 top left) – and the set *S*, while the probability density of the FT uncertainty is reflected in the geometrical path distribution within *S*.

## 3. Results

In this section we describe the experimental setup and give a short summary of corresponding fibre tracking results. An extensive discussion of the results is given in the next section.

For the glioma patient we defined two seed regions, each consisting of $n = 100$ seed points at the level of the cerebral peduncle as well as two destination regions in the precentral gyrus for tracking the fibres of the pyramidal tract. For the healthy volunteer we defined a single small seed region with $n = 20$ mid-sagittally within the posterior part of the corpus callosum. For the pyramidal tract, $m = 5$ was chosen, where *m* denotes the number of how often the FT algorithm is started each with independently generated *variational noise* and for each seed point (cf. Sec. 2.4.2). For the corpus callosum, *m* was set to 10.

### 3.1 Original FT Results vs. Variational Noise

Figure 3 and Figure 4 (upper row) compare the original (superset) FT result with that achieved by adding complex Gaussian noise ($\sigma = 5$ or 10, respectively) to the images. As one can see, this so-called *variational noise* causes a widening and an aggregation of the fibres.

### 3.2 Resolution Effects

We examined the FT result depending on the resolution of the DW images. Before supersampling the images to an isotropic resolution, we downsample them to $4\times4\times4$ mm$^3$ or to $6\times6\times6$ mm$^3$, respectively, also using a three-lobed Lanczos filter. The results can be found in Figure 3 and 4 (middle row), which show that the reconstructed paths are smoothed with decreasing resolution. Moreover, new branchings appear within the reconstruction and others are missed (cf. Fig. 4 middle row).

### 3.3 SNR Effects

We also examined the effect of adding noise to the images. Before supersampling, we added noise of $\sigma = 10$ and $\sigma = 20$ to the images. The corresponding FT results can be found in Figure 3 and 4 (bottom row). Note that the noise leads to a thinning of the reconstructed fibre bundles and only some new false paths are reconstructed. It is remarkable that all important paths are still reconstructed despite of the bad image quality (cf. Fig. 1 bottom center).

<INSERT FIGURES 3 AND 4 HERE>

## 4. Discussion

Our results must be discussed with respect to the anatomical accuracy of diffusion tensor based fibre tracking. Current DTI protocols used for FT yield an effective image resolution of approximately two millimetres, while the acquired SNR represents a trade-off between scan-

ning time and image quality. Due to the limited resolution, only larger white matter tracts can be reconstructed in principle. The anatomical accuracy of a given FT algorithm is related to its sensitivity, i.e. its ability to delineate white matter tracts of a given size and diffusion anisotropy, to its behaviour at branching or crossing fibre bundles, and to its ability to accurately represent the size or width of a given fibre tract. From a neurosurgical perspective, the sensitivity and the size representation are critical as soon as the FT results are used in combination with neuronavigation as a basis for resection guidance (11).

For most figures presented in this paper, we used variational noise with repeated FT under identical starting and boundary conditions in order to demonstrate the uncertainty of FT. When comparing the results with and without variational noise, a systematic widening of the reconstructed fibre tracts can be observed with variational noise. This can be interpreted such that conventional FT tends to avoid the boundary of the white matter tract to be reconstructed and to run towards the centre of the tract. This can be explained by the fact that due to partial volume averaging the diffusion anisotropy is decreased and the main diffusion direction is disturbed at the tract borders. In contrast, after adding variational noise the reconstructed paths are slightly disturbed such that the probability of reaching the tract border increases. After accumulating multiple repetitions with independently generated noise, the overall set of reconstructed paths yield a better representation of the true tract size than without variational noise, even though the seed and target regions as well as the FT parameters are kept constant. As a further effect of accumulating multiple FT repetitions with variational noise, the detection probability of a given fibre branching increases, since more diffusion paths on slightly variable data are reconstructed. Also, we expect that this approach has a higher chance to reconstruct thin and highly curved white matter tracts.

It is instructive to compare the FT results for two types of artificially impaired image quality, first the decrease of image resolution (Figs. 3 and 4 middle row) and second the decrease of SNR (Figs. 3 and 4 bottom row). Decreasing the image resolution yields smoother FT results

as can be easily explained due to omitting the spatial high-frequency content of the image data. The increased path smoothness seems as a benefit at first sight, but also means that in areas of high tract curvature the tracking accuracy is impaired. For instance, the structure of the cortical tips of the reconstructed pyramidal tract are blurred with decreasing image resolution (Fig. 3 middle row). As secondary effects, some paths become much longer while other paths a missed (Fig. 4 middle row). Conversely, decreased SNR yields more wiggly tracked fibre bundles. Still, the boundary of major tracts is more or less constant when compared to the results on the original data set (Fig. 4 bottom row). As secondary effects, some paths are terminated earlier and some false minor branches are reconstructed (Figs. 3 and 4 bottom row). Other than discussed in literature, we find that tract reconstruction is only mildly impaired by increased image noise up to a certain level. While simulations suggest that the path deviation approximately increases linearly with the distance to the seed point (1, 12, 16) we find that the reconstructed tracts do not exceed a given boundary. We argue that this is due to the fact that the anisotropic diffusion pattern contained in the image data does not allow for arbitrary path deviations even though considerable noise was added. Otherwise stated, under average imaging conditions we do not see the danger that the reconstructed tract size is overestimated. Rather, as discussed above, most current approaches are likely to underestimate the tract size.

We did not assess the effects of dedicated noise removal schemes such as proposed by Chen and Hsu (3) and McGraw et al. (17). In an optimal case, however, one could hope that white matter tracts are reconstructed more completely but without removing details of the individual paths as an effect of smoothing.

Moreover, it is surprising how well the pyramidal tracts in the glioma patient were reconstructed even though downsampling the image data to an isotropic resolution of as coarse as 6.0×6.0×6.0 mm³ before FT. We see this as effect both of using a higher-order filter for interpolation of the data before FT and of the properties of the employed extended deflection-based FT algorithm.

We conclude that the presented approach might offer a perspective to overcome the problem of size underestimation observed by current FT approaches. Moreover, the effects of image quality on the tracking result will depend on the employed FT algorithm and must be handled with care. An advantage of the variational noise approach is that it is applicable to any acquired set of diffusion tensor images other than the bootstrap approach that requires individually stored repeated acquisitions. Even though the computation efforts are greatly reduced compared to bootstrapping, future work is required in order to further reduce the required computation time to the order of a few seconds.

Kinoshita et al. state that "further validation of fibre tracking images and the improvement and optimisation of the fibre tracking technique are required" (11). Based on our preliminary findings, we propose to deepen the systematic evaluation of FT applied to major white matter tracts under controlled but realistic imaging conditions in dependency of image resolution, SNR, and pathology. Therein, also newer FT algorithms should be taken into account (e.g. 5, 7, 29). The evaluation on in-vivo images should be complemented by a variety of phantom studies, both physical phantoms that are suitable as a basis for DTI scanning and software phantoms (14, 23), which should be designed to model typical white matter tract configurations under specific imaging conditions with an exactly known ground truth on the modelled anatomy and tissue anisotropy.

## 5. Acknowledgements

We would like to thank Matthias Althaus, Peter Erhard, Olaf Konrad-Verse, Florian Link, Guido Prause, Mathias Schlüter, and Bram Stieltjes for the fruitful discussion and their valuable help. In particular, the employed fibre tracking and visualization methods have been developed by M. Schlüter and O. Konrad-Verse, and the 3T DTI data has been provided by P. Erhard.

## 6. References


1. Anderson AW (2001) Theoretical Analysis of the Effects of Noise on Diffusion Tensor Imaging. Magn Reson Med. 46(6):1174-88
2. Basser PJ, Pajevic S, Pierpaoli C, Duda J, Aldroubi A (2000) In Vivo Fiber Tractography Using DT-MRI Data. Magn Reson Med. 44(4):625-32
3. Chen B, Hsu EW (2005) Noise Removal in Magnetic Resonance Diffusion Tensor Imaging. Magn Reson Med. 54(2):393-401
4. Efron B. (1979) Bootstrap methods: another look at the jackknife. Ann Statist; 7:1-16
5. Gössl C, Fahrmeir L, Pütz B, Auer LM, Auer DP (2002) Fiber Tracking from DTI Using Linear State Space Models: Detectability of the Pyramidal Tract. Neuroimage 16(2):378-88
6. Gudbjartsson H and Patz S (1995) The Rician distribution of noisy MRI data. Magn Reson Med. 34:910–914, 1995
7. Hagmann P, Thiran JP, Jonasson L, Vandergheynst P, Clarke S, Maeder P, Meulib R (2003) DTI mapping of human brain connectivity: statistical fibre tracking and virtual dissection. Neuroimage 19(3):545-54
8. Jones DK (2003) Determining and Visualizing Uncertainty in Estimates of Fiber Orientation From Diffusion Tensor MRI. Magn Reson Med.; 49(1):7-12
9. Jones DK, Pierpaoli C (2005a) Confidence Mapping in Diffusion Tensor Magnetic Resonance Imaging Tractography Using a Bootstrap Approach. Magn Reson Med. 53(5):1143-9
10. Jones DK, Travis AR, Greg G, Pierpaoli C, Basser PJ (2005b) PASTA: Pointwise Assessment of Streamline Tractography Attributes. Magn Reson Med. 53(6):1462-7
11. Kinoshita M, Yamada K, Hashimoto N, Kato A, Izumoto S, Baba T, Maruno M, Nishimura T, Yoshiminie T (2005) Fiber-Tracking does not Accurately Estimate Size of Fiber

Bundle in Pathological Condition: Initial Neurosurgical Experience Using Neuronavigation and Subcortical White Matter Stimulation. Neuroimage 25(2):424-9

12. Lazar M, Alexander AL (2003) An error analysis of white matter tractography methods: synthetic diffusion field simulations. Neuroimage 20(2):1140-53
13. LeBihan D (2003) Looking into the Functional Architecture of the Brain with Diffusion MRI. Nat Rev Neurosci. 4(6):469-80
14. Leemans A, Sijbers J, Verhoye M, Van der Linden A, Van Dyck D. (2005) Mathematical Framework for Simulating Diffusion Tensor MR Neural Fiber Bundles. Magn Reson Med. 53(4):944-53
15. Lin CP, Tseng WYI, Cheng HC, Chen JH (2001) Validation of Diffusion Tensor Magnetic Resonance Axonal Fiber Imaging with Registered Manganese-Enhanced Optic Tracts. Neuroimage 14(5):1035-47
16. Lori NF, Akbudak E, Shimony JS, Cull TS, Snyder AZ, Guillory RK, Conturo TE (2002) Diffusion Tensor Fiber Tracking of Human Brain Connectivity: Acquisition Methods, Reliability Analysis, and Biological Results. NMR Biomed 15(7-8):494-515
17. McGraw T, Vemuri BC, Chen Y, Rao M, Mareci T (2004) DT-MRI Denoising and Neuronal Fiber Tracking. Med Image Anal. 8(2):95-111
18. Mori S, Crain BJ, Chacko VP, van Zijl PCM (1999) Three-Dimensional Tracking of Axonal Projections in the Brain by Magnetic Resonance Imaging. Ann Neurol. 45(2):265-9
19. Nimsky C, Ganslandt O, Hastreiter P, Wang R, Benner T, Sorensen AG, Fahlbusch R (2005a) Intraoperative Diffusion Tensor MR Imaging: Shifting of White Matter Tracts during Neurosurgical Procedures - Initial Experience. Radiology 234(1):218-25
20. Nimsky C, Ganslandt O, Hastreiter P, Wang R, Benner T, Sorensen AG, Fahlbusch R (2005b) Preoperative and Intraoperative Diffusion Tensor Imaging-Based Fiber Tracking in Glioma Surgery. Neurosurgery 56(1):130-7

21. Koch MA, Glauche V, Finsterbusch J, Nolte UG, Frahm J, Weiller C, Buchel C (2002) Distortion-free diffusion tensor imaging of cranial nerves and of inferior temporal and orbitofrontal white matter. Neuroimage; 17(1): 497-506

22. Pajevic S, Basser PJ (1999) Non-parametric statistical analysis of diffusion tensor MRI data using the bootstrap method. 7th Annual Meeting ISMRM, p. 1790

23. Schlüter M, Konrad-Verse O, Hahn HK, Stieltjes B, Rexilius J, Peitgen HO (2005a) White Matter Lesion Phantom for Diffusion Tensor Data and Its Application to the Assessment of Fiber Tracking. In: Medical Imaging 2005, Physiology, Function, and Structure from Medical Images, Proc. SPIE Vol. 5746: 835-844

24. Schlüter M, Stieltjes B, Hahn HK, Rexilius J, Konrad-Verse O, Peitgen HO (2005b) Detection of Tumor Infiltration in White Matter Fiber Bundles Using Diffusion Tensor Imaging. Int J Medical Robotics and Computer Assisted Surgery 1(3): 80-86

25. Schwartz RB, Hsu L, Wong TZ, Kacher DF, Zamani AA, Black PM, Alexander E 3rd, Stieg PE, Moriarty TM, Martin CA, Kikinis R, Jolesz FA (1999) Intraoperative MR Imaging Guidance for Intracranial Neurosurgery: Experience with the first 200 Cases. Radiology; 211(2):477-88

26. Sijbers J, den Dekker AJ, Van Audekerke J, Verhoye M, Van Dyck D. (1998) Estimation of the noise in magnitude MR images Magn Reson Imaging.;16(1):87-90

27. Tournier JD, Calamante F, King MD, Gadian DG, Connelly A. (2002) Limitations and Requirements of Diffusion Tensor Fiber Tracking: An Assessment Using Simulations. Magn Reson Med; 47(4):701-8

28. Weinstein D.M., Kindlmann G.L., Lundberg E.C. (1999). Tensorlines: advection-diffusion based propagation through diffusion tensor fields. IEEEVisualization Proc.; San Fransisco: 249-253

29. Westin CF, Maier SE, Mamata H, Nabavi A, Jolesz FA, Kikinis R. (2002) Processing and visualization for diffusion tensor MRI. Med Image Anal.; 6(2):93-108

30. Yamada K, Kizu O, Mori S, Ito H, Nakamura H, Yuen S, Kubota T, Tanaka O, Akada W, Sasajima H, Mineura K, Nishimura T. (2003) Brain Fiber Tracking with Clinically Feasible Diffusion-Tensor MR Imaging: Initial Experience. Radiology; 227(1):295-301
31. MeVisLab development environment for medical image processing and visualization Version 1.2 (2005); http://www.mevislab.de

## Figures

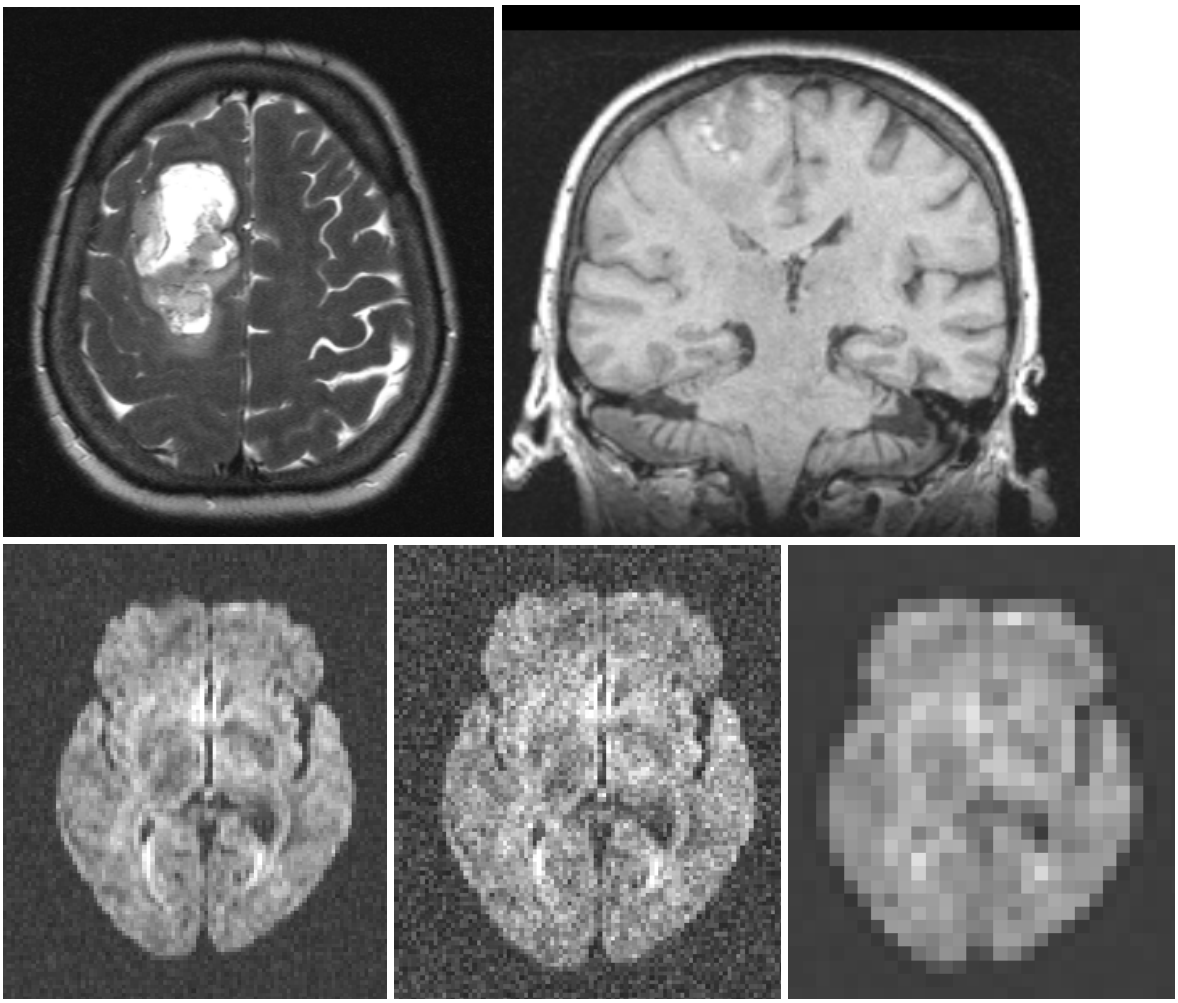

**Figure 1:** MRI data of glioma patient; top left: axial T2 weighted image, top right: coronal T1 weighted image; bottom left: original DTI data (first of six gradient directions, b=1000); bottom center: same as before but additive complex Gaussian noise ($\sigma = 20$, compare to Figs. 3 and 4 bottom right); bottom right: same as bottom left but downsampled to an isotropic resolution of 6×6×6 mm³ (compare to Figs. 3 and 4 middle row, right image).

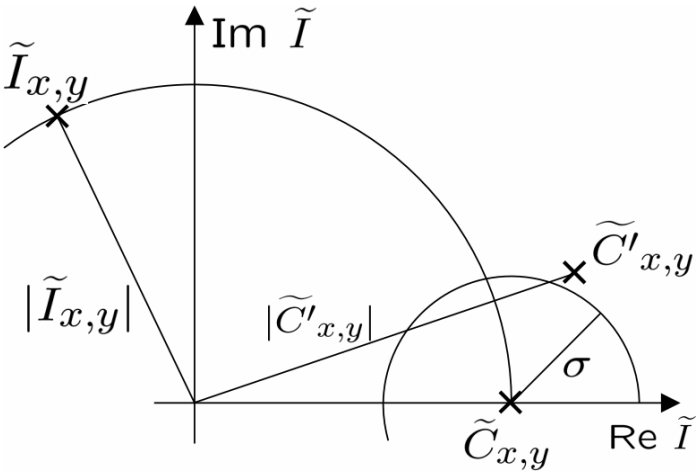


**Figure 2:** Schematic drawing of adding complex Gaussian noise of width $\sigma$ to a pixel value $|\widetilde{I}_{x,y}|$ of the magnitude image with corresponding complex number $\widetilde{C}_{x,y}$ . The new magnitude value is denoted as $|\widetilde{C'}_{x,y}|$.

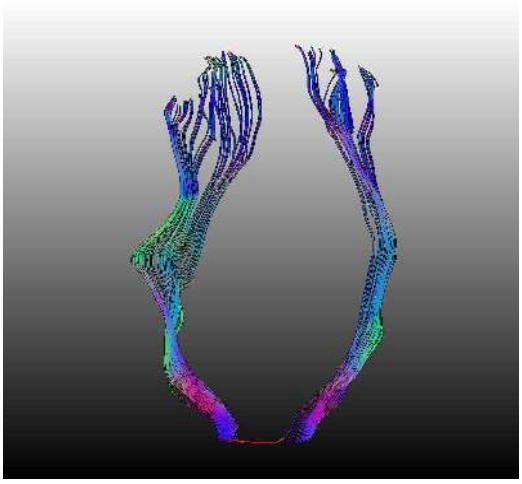

no variational noise

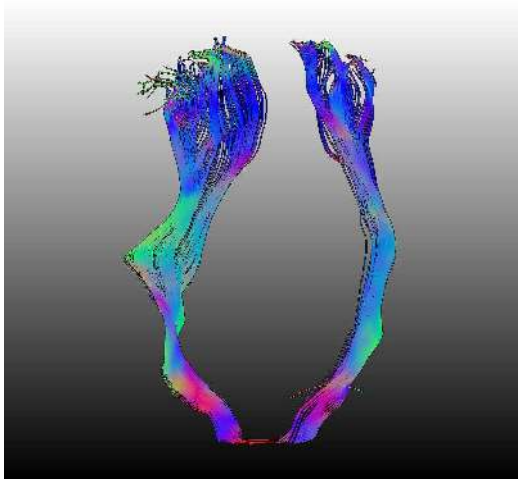

variational noise ($\sigma = 5$)

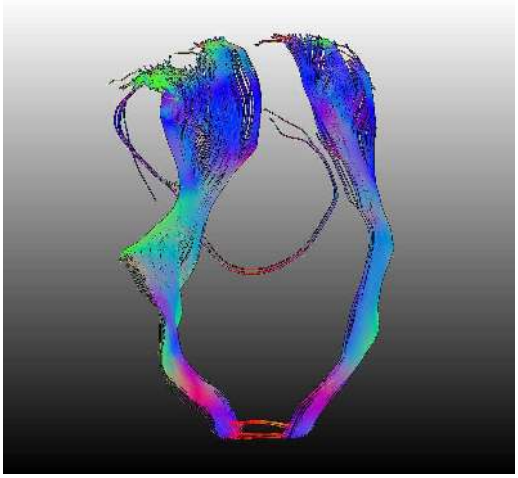

downsampling (4×4×4 mm³) and variational noise ($\sigma = 5$)

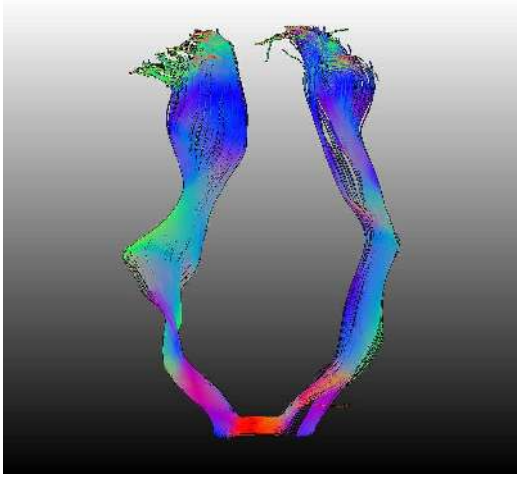

downsampling (6×6×6 mm³) and variational noise ($\sigma = 5$)

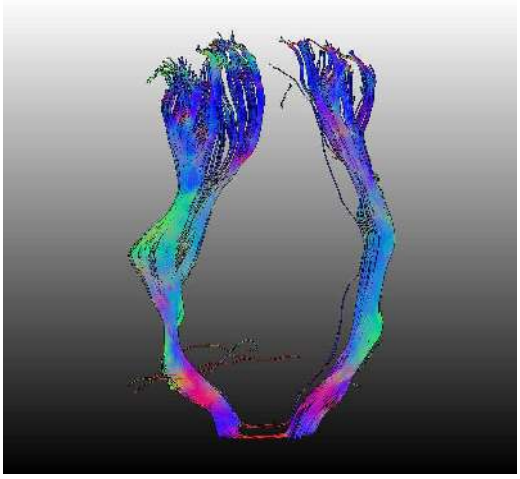

additional basic noise ($\sigma = 10$) and variational noise ($\sigma = 5$)

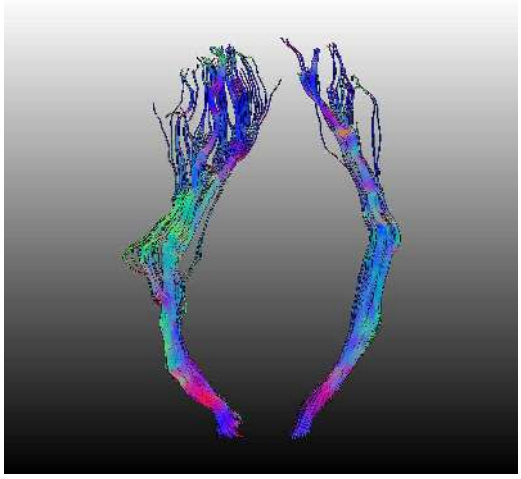

additional basic noise ($\sigma = 20$) and variational noise ($\sigma = 5$)

**Figure 3**: Visualization of FT uncertainty for different resolutions and levels of noise for the pyramidal tract. Before tracing, all data sets were supersampled to 1.5×1.5×1.5 mm³ using a three-lobed Lanczos filter.

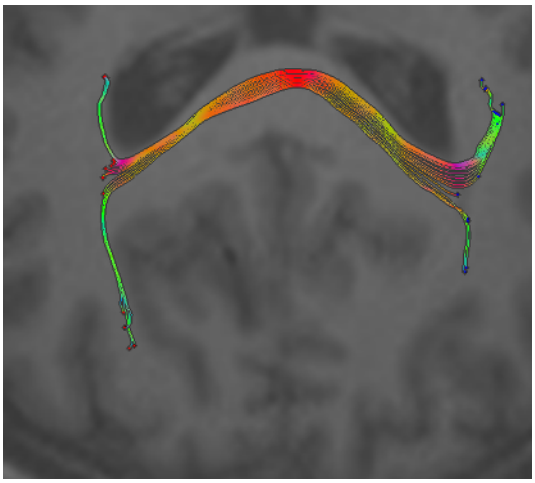

no variational noise

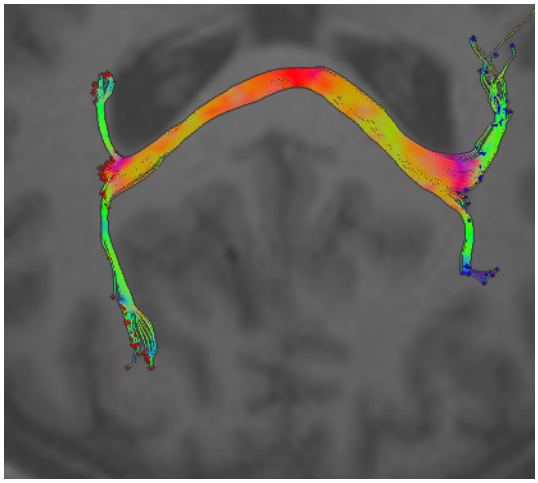

variational noise ($\sigma$ = 10)

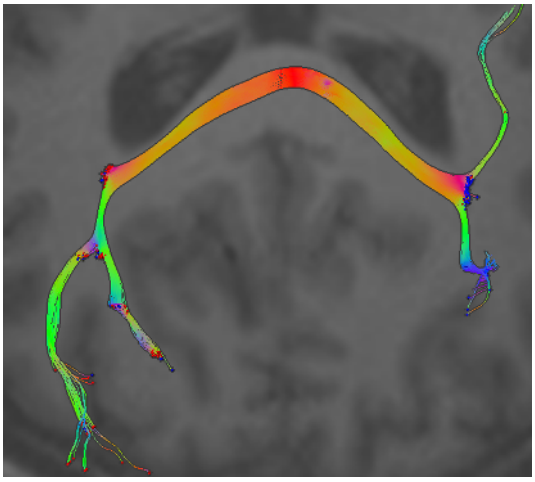

downsampling (4×4×4 mm³) and variational noise ($\sigma$ = 10)

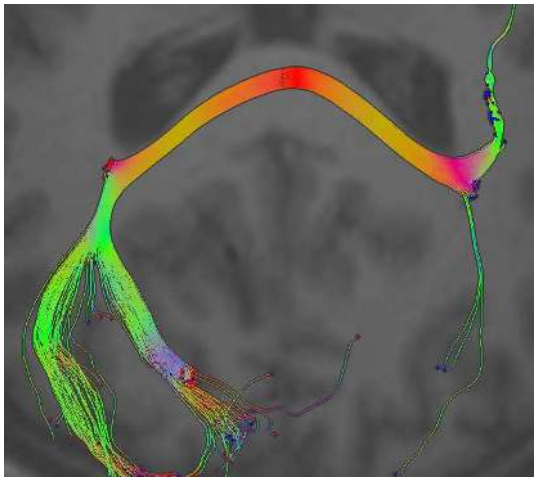

downsampling (6×6×6 mm³) and variational noise ($\sigma$ = 10)

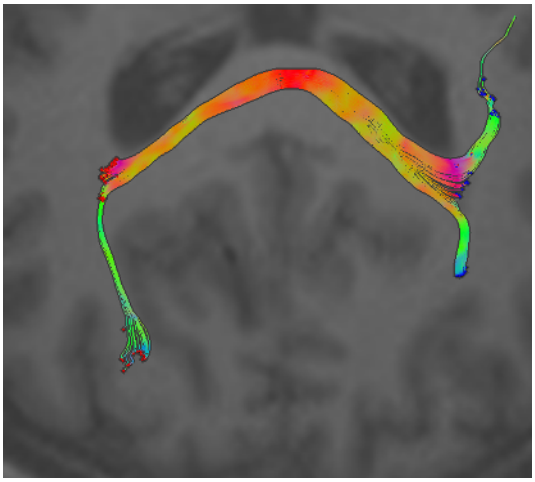

additional basic noise ($\sigma$ = 10) and variational noise ($\sigma$ = 10)

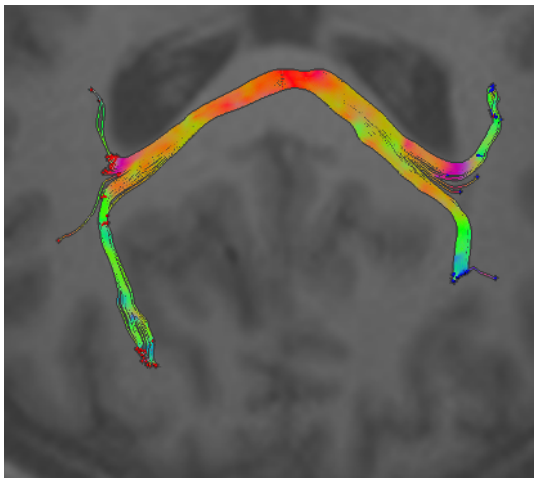

additional basic noise ($\sigma$ = 20) and variational noise ($\sigma$ = 10)

**Figure 4**: Visualization of FT uncertainty for different resolutions and levels of noise for a seed region within the corpus callosum. Before tracing, all data sets were supersampled to 1.5×1.5×1.5 mm³ using a three-lobed Lanczos filter.